Metrol. Meas. Syst., Vol. 26 (2019) No. 4, pp. 595–605
DOI: 10.24425/mms.2019.130561

METROLOGY AND MEASUREMENT SYSTEMS
Index 330930, ISSN 0860-8229
www.metrology.pg.gda.pl

REDUCED-COST DESIGN CLOSURE OF ANTENNAS BY MEANS OF GRADIENT SEARCH WITH RESTRICTED SENSITIVITY UPDATE

Sławomir Kozieł[1, 2)], Anna Pietrenko-Dąbrowska[2)]

1) *Reykjavik University, Engineering Optimization and Modeling Center, Menntavegur 1, 101 Reykjavik, Iceland* (✉ *koziel@ru.is*, +35 45 996 376)
2) *Gdańsk University of Technology, Faculty of Electronics, Telecommunications and Informatics, G. Narutowicza 11/12, 80-233 Gdańsk, Poland* (*anna.dabrowska@pg.edu.pl*)

Abstract

Design closure, *i.e.*, adjustment of geometry parameters to boost the performance, is a challenging stage of antenna design process. Given complexity of contemporary structures, reliable parameter tuning requires numerical optimization and can be executed using local algorithms. Yet, EM-driven optimization is a computationally expensive endeavour and reducing its cost is highly desirable. In this paper, a modification of the trust-region gradient search algorithm is proposed for accelerated optimization of antenna structures. The algorithm is based on sparse updates of antenna sensitivities involving various methods that include the Broyden formula used for selected parameters, as well as dimensionality- and convergence-dependent acceptance thresholds which enable additional speedup, and make the procedure easy to tune for various numbers of antenna parameters. Comprehensive verification executed for a set of benchmark antennas delivers consistent results and considerable cost reduction of up to 60 percent with respect to the reference algorithm. Experimental validation is also provided.

Keywords: antenna design, design closure, EM-driven optimization, gradient search, sensitivity update.

1. Introduction

Design of antenna structures is a multi-stage process. One of its steps is the development of antenna topology, normally dictated by a combination of performance specifications imposed upon the system (*e.g.*, wideband [1], multi-band [2]), particular functionalities to be implemented (*e.g.*, circular polarization [3], band notches [4], MIMO [5], *etc.*), and constraints (*e.g.*, maximum allowed footprint area [6]). The last stage is a design closure, *i.e.*, adjustment of antenna parameters, aimed at improving its performance figures. The role of this stage has been increasing over the years because traditional design methods (*e.g.*, involving the low-level antenna theory [7]) are not applicable to majority of contemporary structures due to their geometrical complexity. A good example are compact antennas, reliable evaluation of which require full-wave *electromagnetic* (EM) analysis to account for the coupling effects between tightly arranged components [8, 9].

Conventional design closure approaches, mostly experience-driven parameter sweeping, are still widely used in antenna community; however, their relevance has been declining for several reasons. These include the need for handling highly-dimensional parameter spaces, multiple performance figures and constraints [10]. Neither can be effectively controlled by varying one or two parameters at a time. Rigorous numerical optimization is a much more reliable approach [11, 12], yet it is challenging primarily due to its high cost, especially when global search is required [13, 14]. Among various methods developed to address this issue, making use of adjoined sensitivities [15] (local optimization), machine learning techniques [16] (global optimization), and surrogate-assisted methods [17], seems to be the most promising. The last group of techniques has been attracting much attention recently which is due to an impressive computational speedup that can be achieved when the algorithm is properly tailored to the design problem at hand. The primary acceleration factor here is a surrogate model, a fast representation of the structure under design, which can be constructed as a data-driven (approximation) model (*e.g.*, kriging [18], Gaussian process regression [19]) or physics-based one (space mapping [20], adaptive response scaling [21], manifold mapping [22], feature-based optimization [23]) or a combination of them [24]. It should be noted that – due to the lack of alternatives – physics-based models of antennas are normally developed from coarse-mesh EM simulations [17]. As a consequence, reducing the number of EM analyses during the surrogate model optimization is just as important as for direct optimization.

In this paper, a novel variation of the trust-region gradient search algorithm is proposed that aims at expediting the (local) optimization process of antennas. The procedure can be used for direct optimization of high-fidelity EM models or within the surrogate-assisted procedures involving variable-fidelity simulations. The proposed approach is based on sparse updates of antenna sensitivities involving several mechanisms that include the rank-one Broyden formula applied to selected columns of the Jacobian matrix, as well as adaptive schemes that control the balance between the various sensitivity updating means. These are dependent on both the algorithm convergence status (to achieve additional speedup when close to algorithm termination), and search space dimensionality (to facilitate adjustment of the algorithm control parameters for antenna structures described by various numbers of parameters). The presented methodology is demonstrated using a benchmark set of three antennas. The obtained computational savings are up to sixty percent as compared with the reference algorithm. More importantly, the algorithm performance is consistent with respect to the initial design as indicated through statistical analysis. Experimental validation of selected optimized designs is also provided.

2. Benchmark antennas and design-closure task

The optimization algorithm proposed in this paper will be validated using several wideband antenna structures shown in Fig. 1. All antennas are implemented on RO4350 substrate ($\varepsilon_r = 3.48$, $h = 0.762$ mm). Antenna I ([25], Fig. 1a) is a uniplanar dual-band dipole fed by a *coplanar waveguide* (CPW). The variables are: $\boldsymbol{x} = [l_1\ l_2\ l_3\ w_1\ w_2\ w_3]^T$, whereas $l_0 = 30$, $w_0 = 3$, $s_0 = 0.18$ and $o = 5$ are fixed (all dimensions in mm). Antenna II ([26], Fig. 1b) is a wideband structure described by $\boldsymbol{x} = [L_0\ dR\ R\ r_{rel}\ dL\ dw\ L_g\ L_1\ R_1\ dr\ c_{rel}]^T$. Finally, Antenna III (Fig. 1c), based on the structure of [27], involves 13 design variables $\boldsymbol{x} = [L_0\ L_1\ L_2\ L\ dL\ L_g\ w_1\ w_2\ w\ dw\ L_s w_s c]^T$. The computational models are implemented in CST Microwave Studio and evaluated using its transient solver. For all antennas, the models incorporate the SMA connectors. The structures have been selected to analyse the algorithm performance in search spaces of various

Metrol. Meas. Syst., Vol. 26 (2019), No. 4, pp. 595–605
DOI: 10.24425/mms.2019.130561

dimensionalities. Antenna I is supposed to operate at the centre frequencies of 3 GHz and 5.5 GHz with 8-percent fractional bandwidth. Antennas II and III operate in UWB frequency range (3.1 GHz to 10.6 GHz).

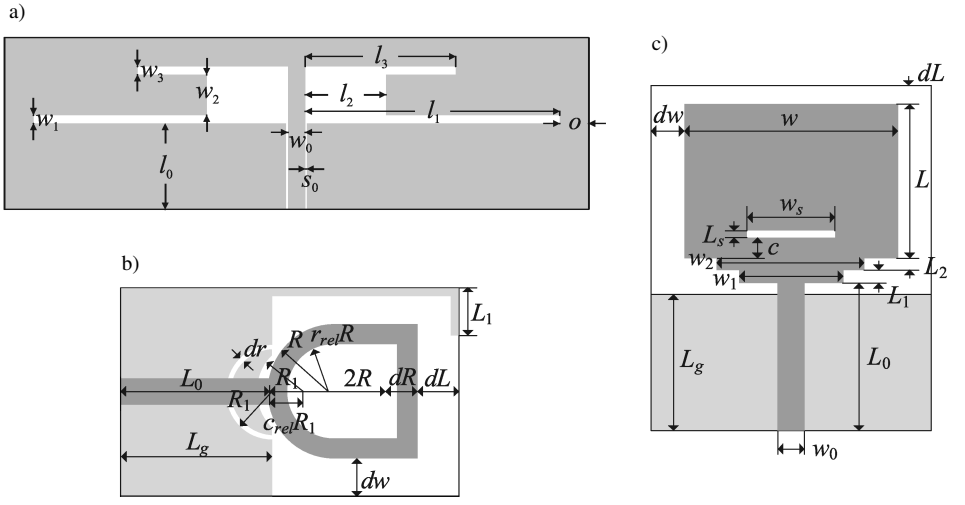

Fig. 1. Antenna structures used for benchmark purposes: a) Antenna I [25]; b) Antenna II [26]; c) Antenna III [27]. Ground plane is marked with light grey shade.

The design closure problem is formulated as a minimization task of the form:

$$\boldsymbol{x}^* = \arg\min_{\boldsymbol{x}} U(\boldsymbol{R}(\boldsymbol{x})), \tag{1}$$

where U is an objective function, and $\boldsymbol{R}(\boldsymbol{x})$ represents the EM-simulated antenna response.

Clearly, a particular definition of the objective function depends on the selected performance figures of interest but also on the imposed design constraints. Here, two types of problems are considered. The first one (for Antennas I through III) is the minimization of the maximum in-band reflection $|S_{11}(\boldsymbol{x},f)|$($f$ stands for frequency). Consequently, we have:

$$U(\boldsymbol{R}(\boldsymbol{x})) = \max_{f\in F} |S_{11}(\boldsymbol{x}, f)|, \tag{2}$$

in which F is the frequency range of interest. Note that the problem (1), (2) is formulated in a minimax sense.

The second type of problem is the maximization of the average in-band gain $G(\boldsymbol{x})$ while maintaining $S(\boldsymbol{x}) \leq -10$ dB, where $S(\boldsymbol{x})$ is the maximum in-band reflection. For this problem (considered for Antenna I), the following objective is used:

$$U(\boldsymbol{R}(\boldsymbol{x})) = -G(\boldsymbol{x}) + \gamma \max\{(S(\boldsymbol{x}) + 10)/10, 0\}^2. \tag{3}$$

Here, the primary objective is the negative average gain, whereas the second part of (3) is a penalty term enforcing satisfaction of the reflection constraint; $\gamma = 10$ is a penalty coefficient with the value selected to ensure noticeable contribution of a penalty term if a violation of the constraint exceeds a fraction of dB. In the case of multiple objectives, a common practice is to select a primary objective and cast others into constraints that can be handled implicitly with

the use of penalty functions. The choice of a penalty coefficient value is of certain importance. Adopting too small a value of γ would lead to yielding an infeasible design (from the point of view of the reflection constraint). If γ value is too high, the steepness of the objective function in the vicinity of the feasible region boundary would lead to problems related to the numerical noise inherent to EM simulation results, thus often resulting in premature algorithm termination (*e.g.*, due to the reduction of the trust region size).

3. Optimization routine: local gradient search with restricted sensitivity updates

In this section, we outline the reference *trust-region* (TR) algorithm, as well as present the concept and implementation of the proposed procedure based on sparse updates of antenna sensitivities. The conventional TR embedded gradient-search algorithm [28] is a suitable method for solving (1) with the objective function described either by (2) or (3) and evaluated through EM analysis with a certain level of numerical noise incorporated. In each iteration of the TR algorithm, an approximation $\boldsymbol{x}^{(i)}$, $i = 0, 1, \ldots$, to the optimum design $\boldsymbol{x}^*$ is obtained by solving:

$$\boldsymbol{x}^{(i+1)} = \arg \min_{\boldsymbol{x};\ -\boldsymbol{d}^{(i)} \le \boldsymbol{x}-\boldsymbol{x}^{(i)} \le \boldsymbol{d}^{(i)}} U(\boldsymbol{L}^{(i)}(\boldsymbol{x})), \tag{4}$$

where a linear approximation $\boldsymbol{L}^{(i)}(\boldsymbol{x}) = \boldsymbol{R}(\boldsymbol{x}^{(i)}) + \boldsymbol{J}_{\boldsymbol{R}}(\boldsymbol{x}^{(i)}) \cdot (\boldsymbol{x} - \boldsymbol{x}^{(i)})$ of $\boldsymbol{R}$ at $\boldsymbol{x}^{(i)}$ is adopted. The TR region size vector is denoted by $\boldsymbol{d}^{(i)}$, and its components are proportional to the parameter ranges. This is to address the issue of significantly different ranges of parameters, a situation commonly occurring in antenna design. In fact, the transmission line component widths and spaces between the lines are typically fractions of millimetres, whereas the transmission line lengths or the dimensions of the substrate/ground planes reach up to tens of millimetres [15]. Thus, a hypercube-like search region, defined as $-\boldsymbol{d}^{(i)} \le \boldsymbol{x} - \boldsymbol{x}^{(i)} \le \boldsymbol{d}^{(i)}$ with the inequalities understood component-wise, is used, instead of an Euclidean ball $\|\boldsymbol{x} - \boldsymbol{x}^{(i)}\| \le d^{(i)}$ usually employed by the TR algorithms. Establishing the initial size vector proportional to the design space sizes enables to treat in a similar way the variables of considerably different ranges. This makes possible avoiding variable scaling, otherwise necessary to ensure that the parameters are of comparable magnitude, which is required for the trust-region algorithm to converge [28]. The TR region size is adjusted complying with the standard rules.

Usually, the Jacobian $\boldsymbol{J}_{\boldsymbol{R}}$ is estimated through *finite differentiation* (FD), hence additional n EM analyses per algorithm iteration are performed (n stands for the number of the design parameters). Applying the Broyden formula, which does not require performing any additional EM analyses, permits to avoid this cost. The proposed algorithm adopts a sparse scheme of Jacobian updates based on the rank-one *Broyden formula* (BF) [29]:

$$\boldsymbol{J}_{\boldsymbol{R}}^{(i+1)} = \boldsymbol{J}_{\boldsymbol{R}}^{(i)} + \frac{\left(\boldsymbol{f}^{(i+1)} - \boldsymbol{J}_{\boldsymbol{R}}^{(i)} \cdot \boldsymbol{h}^{(i+1)}\right) \cdot \boldsymbol{h}^{(i+1)^T}}{\boldsymbol{h}^{(i+1)^T} \boldsymbol{h}^{(i+1)}}, \tag{5}$$

where $\boldsymbol{f}^{(i+1)} = \boldsymbol{R}(\boldsymbol{x}^{(i+1)}) - \boldsymbol{R}(\boldsymbol{x}^{(i)})$, and $\boldsymbol{h}^{(i+1)} = \boldsymbol{x}^{(i+1)} - \boldsymbol{x}^{(i)}$ describes design relocation between subsequent iterations. The alignment between the design relocation direction $\boldsymbol{h}^{(i+1)}$ and the coordinate system axes are used to select the Jacobian columns that are to be updated with BF (*cf.* 5). Here, the alignment threshold value is associated both with the dimensionality of the design space, as well as with the algorithm convergence status measured by the TR region size. The details of the adopted procedure are described below.

Metrol. Meas. Syst., Vol. 26 (2019), No. 4, pp. 595–605
DOI: 10.24425/mms.2019.130561

In the first iteration, the initial estimate of the Jacobian $\boldsymbol{J_R}$ is obtained entirely with FD. In the next iterations, however, for each parameter $k = 1, \ldots, n$, the choice between FD and BF is made depending on a binary selection vector $\boldsymbol{r}^{(i)} = [r_1^{(i)} \ldots r_n^{(i)}]^T$. The FD is performed if $r_k^{(i)} = 1$, while $r_k^{(i)} = 0$ indicates the use of BF. The Jacobian matrix $\boldsymbol{J_R}$ incorporates columns $\boldsymbol{J}_k$ calculated either with FD or BF, where $\boldsymbol{J}_k = \partial \boldsymbol{R}/\partial x_k$ denotes the antenna response sensitivities with respect to the k-th parameter.

In each iteration, a candidate design $\boldsymbol{x}_{tmp}$ is obtained by solving (4) and $\rho = (U(\boldsymbol{R}(\boldsymbol{x}_{tmp}) - U(\boldsymbol{R}(\boldsymbol{x}^{(i)})/(\boldsymbol{L}^{(i)}(\boldsymbol{x}_{tmp}) - \boldsymbol{L}^{(i)}(\boldsymbol{x}^{(i)}))$ *i.e.*, the gain ratio, is calculated. The selection vector $\boldsymbol{r}^{(i+1)}$ for the next iteration is subsequently altered. In the case of a successful iteration ($\rho > 0$), the candidate design $\boldsymbol{x}_{tmp}$ is accepted. Let us denote as $\boldsymbol{e}^{(k)} = [0 \ \ldots \ 0 \ 1 \ 0 \ \ldots \ 0]^T$ (with 1 on the k-th position) the standard basis vectors. The following alignment factors are defined:

$$\varphi_k^{(i+1)} = \left| h^{(i+1)^T} e^{(k)} \right| \Big/ \left\| h^{(i+1)} \right\|. \tag{6}$$

The entries of the selection vector $\boldsymbol{r}^{(i+1)}$ are inferred from the factors as follows: $r_k^{(i+1)} = 0$, if $\varphi_k^{(i+1)}$ is above a user-specified threshold value $0 \leq \varphi_{\min} \leq 1$, otherwise $r_k^{(i+1)} = 1$. The alignment threshold is a control parameter of the algorithm and regulates the use of BF: the greater its value, the more frequently FD is performed. At the same time, a design of a better quality might be obtained. On the other hand, lowering the value of $\varphi_{\min}$ enables to achieve higher computational savings. It is noteworthy, that the alignment factor $\varphi_k^{(i+1)}$ is equal to 1 if the design relocation vector $\boldsymbol{h}^{(i+1)}$ and $\boldsymbol{e}^{(k)}$ are co-linear, whereas $\varphi_k^{(i+1)} = 0$ if they are orthogonal.

As the algorithm converges, the alignment acceptance threshold is adaptively reduced, making possible more frequent replacement of FD by BF. In consequence, a further decrease of the number of EM simulations required to obtain the optimum design is achieved. In the course of the optimization process, the algorithm convergence is described by diminishing TR region size $\delta^{(i+1)} = \|\boldsymbol{d}^{(i+1)}\|$. If it becomes smaller than a user-defined value δ_0, φ starts to decrease according to the following formula:

$$\varphi = \varphi_{\min} \left(\left(\log \left(\left\| \delta^{(i+1)} \right\| / \varepsilon \right) \right) \Big/ \left(\log \left(\|\delta_0\| / \varepsilon \right) \right) \right), \tag{7}$$

where ε stands for the termination threshold for convergence in argument ($\|\boldsymbol{x}^{(i+1)} - \boldsymbol{x}^{(i)}\| < \varepsilon$). Reduction of φ leads to a less stringent condition for using BF and encourages higher computational savings. A remark should be made that the particular form of (7) ensures that as the TR region size approaches ε, φ approaches 0. Hence, it enables even more frequent use of the BF close to the algorithm termination.

The case of a rejected iteration should also be discussed. If it was unsuccessful, *i.e.*, $\rho < 0$, the candidate design $\boldsymbol{x}_{tmp}$ is discarded, however, prior to the rejection, it is used to guide the optimization process by enhancing the Jacobian $\boldsymbol{J_R}$ [29]. First, the temporary estimate of the Jacobian $\boldsymbol{J_R}(\boldsymbol{x}_{tmp})$ is obtained solely using BF. Then, temporary decision factors $\varphi_k^{(i)}$ are calculated for each antenna parameter: if a given factor $\varphi_k > \varphi_{\min}$, the respective column of temporary Jacobian $\boldsymbol{J}_k(\boldsymbol{x}_{tmp})$ is substituted for the corresponding column of $\boldsymbol{J}_k(\boldsymbol{x}^{(i-1)})$ from the previous iteration.

In this paper, the acceptance threshold φ value is associated with the design space dimensionality, which is a way of making the adjustment of the algorithm control parameters dimensionality-independent. Instead of appointing a specific threshold value, we assign a value for which the expected percentage of Jacobian columns would be updated using BF. In order to do so, a statistical analysis is necessary for any given dimensionality n. The acceptance threshold φ_p for which

the expected percentage p [%] directions will be updated using (4) is calculated as:

$$\varphi_p = \arg\min_{\varphi} \left| \frac{p}{100} - N_p^{-1} \sum_{j=1}^{N_p} \sum_{k=1}^{n} \left\lceil \beta_{j.k} - \varphi \right\rceil \right|, \tag{8}$$

where N_p denotes the number of random observations $\boldsymbol{y}^{(j)}$, $j = 1, \ldots, N_p$, and factors $\beta_{j.k} = |\boldsymbol{y}^{(k)T} \boldsymbol{e}^{(k)}| / \|\boldsymbol{y}^{(k)}\|$, for all j and $k = 1, \ldots, n$. The percentage of directions, for which the alignment coefficient is higher than φ, is minimized using the pattern search algorithm (as a finite set of observations is used, the cost function is noisy). By employing (8), the threshold becomes related only to the desired value of the percentage p (*cf.* Fig. 2). The results presented in Section 4 indicate versatility of the proposed approach for antenna structures described by various numbers of parameters.

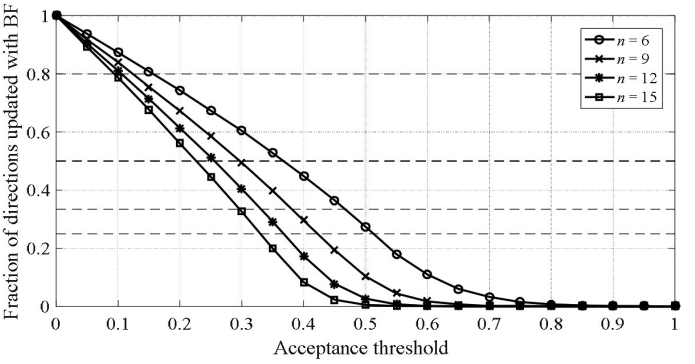

Fig. 2. The expected fraction of directions with Jacobian updated using BF versus the acceptance threshold value for various parameter space dimensionalities. Note considerable differences in the threshold values ensuring the same percentage.

4. Results

Antennas I through III have been optimized using the algorithm of Section 3. For Antenna I, two cases were considered: the best matching design (*cf.* (2)) and the maximum gain design (*cf.* (3)). In order to gather statistical data on the algorithm performance, ten optimization runs have been executed using random initial designs.

The results are presented in Tables 1 and 2. Fig. 3 shows representative antenna responses. The standard TR algorithm (4) has been used as a reference. It should be emphasized that the topic of the paper is direct optimization, therefore comparisons with *surrogate-based optimization* (SBO) techniques, *e.g.*, [20–23], or specialized algorithms for antenna miniaturization (*e.g.*, [24]) are of no relevance here.

The lower and upper bounds for design variables of uniplanar dual-band dipole (Antenna I) are the following: $\boldsymbol{l} = [15.0\ 5.0\ 5.0\ 0.2\ 0.5\ 0.5]^T$, and $\boldsymbol{u} = [50.0\ 20.0\ 30.0\ 0.6\ 5.0\ 5.0]^T$. For Antenna II, the lower and upper bounds are: $\boldsymbol{l} = [4.0\ 0\ 3.0\ 0.1\ 0\ 0\ 4.0\ 0\ 2.0\ 0.2\ 0.2]^T$, and $\boldsymbol{u} = [15.0\ 6.0\ 8.0\ 0.9\ 5.0\ 8.0\ 15.0\ 6.0\ 5.0\ 1.0\ 0.9]^T$, whereas for Antenna III they are: $\boldsymbol{l} = [5.0\ 0.1\ 0.1\ 5.0\ 0\ 5.0\ 0.1\ 0.1\ 5.0\ 0\ 0.01\ 0.1\ 0.1]^T$, and $\boldsymbol{u} = [20.0\ 2.0\ 3.0\ 20.0\ 5.0\ 20.0\ 1.0\ 1.0\ 25.0\ 10.0\ 0.2\ 0.9\ 0.3]^T$.

Metrol. Meas. Syst., Vol. 26 (2019), No. 4, pp. 595–605
DOI: 10.24425/mms.2019.130561

Table 1. Optimization results for Antenna I.

		Optimization for best matching					Optimization for maximum gain				
Method		Cost[1]	Savings[2] [%]	max $\|S_{11}\|$[3] [dB]	$\Delta\|S_{11}\|$[4] [dB]	STD[5] [dB]	Cost[1]	Savings[2] [%]	Gain[6] [dB]	Δ Gain[7] [dB]	STD[8] [dB]
Reference		72.6	–	−11.6	–	0.3	80.3	–	4.0	–	0.09
This work p	66%	49.9	31.3	−11.5	0.1	0.2	59.9	25.4	3.9	0.08	0.15
	83%	42.2	41.9	−11.3	0.3	0.7	33.2	58.7	3.8	0.15	0.19
	90%	37.9	47.8	−11.1	0.5	1.1	29.3	63.5	3.8	0.16	0.17
	95%	34.1	53.0	−10.8	0.8	1.6	30.4	62.1	3.8	0.21	0.21
	98%	36.2	50.1	−10.8	0.8	1.3	24.8	69.1	3.7	0.28	0.23
	100%[$]	27.2	62.5	−10.7	0.9	1.5	24.8	69.1	3.7	0.29	0.24

[1] Number of EM simulations averaged over 10 algorithm runs;
[2] Percentage-wise cost savings w.r.t. the reference algorithm;
[3] Maximum in-band reflection S_{11} in dB;
[4] Degradation of S_{11} w.r.t. the reference algorithm in dB;
[5] Standard deviation of S_{11} in dB across 10 algorithm runs (random initial points);
[6] Maximum in-band gain G in dB;
[7] Degradation of gain G w.r.t. the reference algorithm in dB;
[8] Standard deviation of G in dB across 10 algorithm runs (random initial points);
[$] Broyden-only Jacobian updates (no FD used).

Table 2. Optimization results for Antennas II and III.

		Antenna II					Antenna III				
Method		Cost[1]	Savings[2] [%]	max $\|S_{11}\|$[3] [dB]	$\Delta\|S_{11}\|$[4] [dB]	STD[5] [dB]	Cost[1]	Savings[2] [%]	Gain[6] [dB]	Δ Gain[7] [dB]	STD[8] [dB]
Reference		111.2	–	−14.9	–	0.6	139.7	–	−17.6	–	1.5
This work p	66%	72.7	34.6	−14.3	0.6	0.8	82.3	41.1	−15.4	2.2	2.3
	83%	54.0	51.4	−13.9	1.0	0.9	69.1	50.5	−15.9	1.7	2.5
	90%	47.9	56.9	−13.8	1.1	1.0	51.3	63.3	−15.1	2.5	3.3
	95%	41.2	62.9	−14.2	0.7	1.1	45.5	67.4	−14.6	3.0	4.4
	98%	33.0	70.3	−13.7	1.2	1.1	34.2	75.5	−14.4	3.2	4.8
	100%[$]	26.5	76.2	−13.5	1.4	1.2	34.3	75.4	−13.7	3.9	3.9

[1] Number of EM simulations averaged over 10 algorithm runs;
[2] Percentage-wise cost savings w.r.t. the reference algorithm;
[3] Maximum in-band reflection S_{11} in dB;
[4] Degradation of S_{11} w.r.t. the reference algorithm in dB;
[5] Standard deviation of S_{11} in dB across 10 algorithm runs (random initial points);
[$] Broyden-only Jacobian updates meaning no FD used whatsoever.

The data in Tables 1 and 2 clearly indicate computational benefits of the proposed algorithm which are more pronounced with the increasing value of the acceptance threshold p. Note that 100% refers to the pure Broyden algorithm with no FD updates. It is only given for comparison purposes, as the design quality obtained with the sole use of BF is poor. At the same time, the algorithm reliability is affected by the percentage value p which can be observed through the increasing deviation of the average objective function value with respect to the reference algorithm as well as an increasing standard deviation of the objective function. Importantly, the dependence of the results on p is very much consistent for all four cases and p = 90% can be

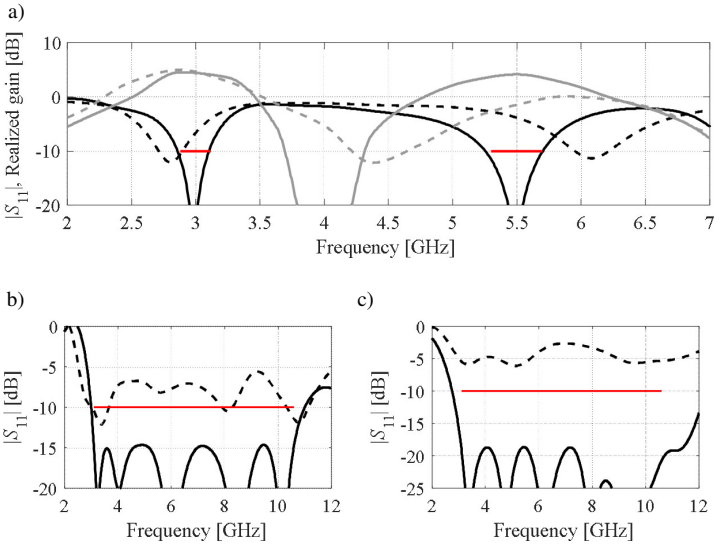

Fig. 3. Reflection characteristics for representative algorithm runs: a) Antenna I (the realized gain characteristics are shown in grey); b) Antenna II; c) Antenna III. Horizontal lines mark the design specifications (the intended operating band); (- - -) initial design, (—) optimized design.

considered an optimum value for which the savings are high (58% on average) while reliability is still acceptable as compared with the reference. This consistency, achieved for design spaces from six to thirteen parameters, is a result of introducing a dimensionality-dependent acceptance threshold (*cf.* Section 3). The standard deviation employed as a measure of the result repeatability is the smallest for the reference algorithm and increases with p. However, it is also growing with the parameter space dimension, which has nothing to do with the quality of the optimization algorithm but rather with the fact that different local optima are attained in each run due to random starting points. The number and variety of these optima clearly increase with the number of antenna parameters and so is the standard deviation. It should be reiterated at this point that the considered algorithm is a local one: identifying a globally optimal design is neither possible nor sought for in this work.

Selected designs of Antennas I through III have been fabricated and measured. Fig. 4 shows photographs of the antenna prototypes, whereas Figs. 5 through 6 illustrate comparison of simulated and measured reflection responses, realized gain characteristics, as well as H-plane radiation patterns. The agreement between simulated and measured responses is satisfactory.

Fig. 4. Photographs of the fabricated prototypes of Antennas I through III optimized using the proposed algorithm: a) Antenna I (gain optimization); b) Antenna II; c) Antenna III.

Metrol. Meas. Syst., Vol. 26 (2019), No. 4, pp. 595–605
DOI: 10.24425/mms.2019.130561

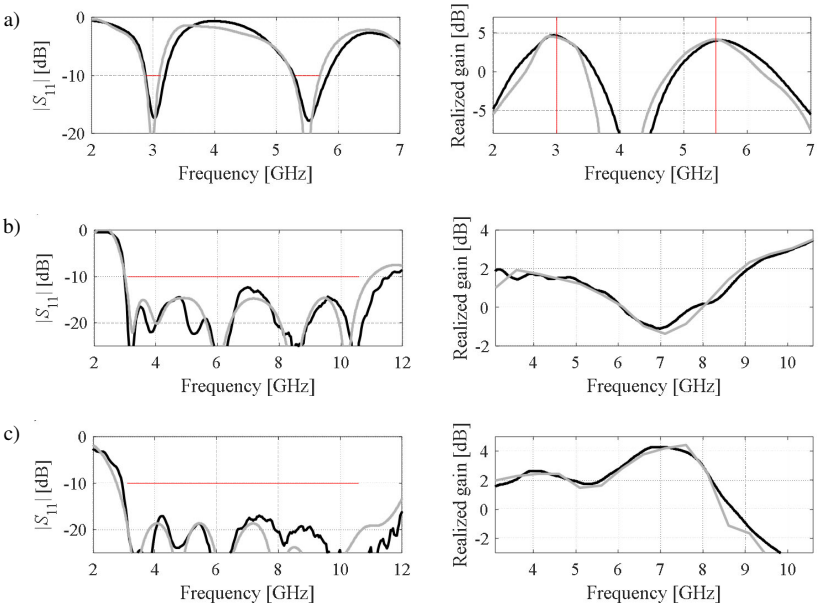

Fig. 5. Simulated (grey) and measured (black) reflection and (broadside) achieved gain characteristics: a) Antenna I; b) Antenna II; c) Antenna III.

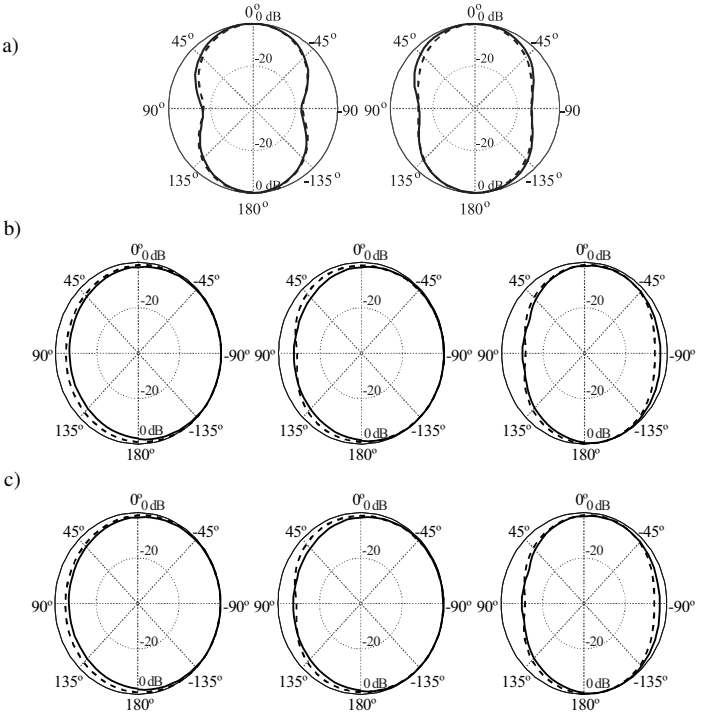

Fig. 6. Simulated (- - -) and measured (—) H-plane radiation patterns: a) Antenna I (at 3 GHz and 5.5 GHz); b) Antenna II; c) Antenna III. The plots in (b) and (c) are, from left to right, for 4 GHz, 6 GHz, and 8 GHz, respectively.

5. Conclusions

The paper proposes a novel TR algorithm with restricted sensitivity updates for antenna optimization. Comprehensive validation, also performed in a statistical sense, demonstrated considerable computational savings that can be obtained, with the trade-off between the speed-up and the design quality conveniently controlled using one parameter, the acceptance threshold for Broyden-based updates. As the latter is made dimensionality-dependent, the consistency of results is achieved for antenna structures of various numbers of geometry parameters. Potential applications of the algorithm include expedited direct optimization of antennas as well as solving sub-problems within variable-fidelity surrogate-assisted frameworks.

Acknowledgements

This work was supported in part by the Icelandic Centre for Research (RANNIS) Grant 174114051 and 174573052, and by the National Science Centre of Poland Grant 2015/17/B/ST6/01857. The authors would like to thank Dassault Systemes, France, for making CST Microwave Studio available.

References

[1] Saini, R.K., Dwari S. (2016). A broadband dual circularly polarized square slot antenna. *IEEE Trans. Ant. Prop.*, 64(1), 290–294.

[2] Liao, W.J., Hsieh, C.Y., Dai, B.Y., Hsiao, B.R. (2015). Inverted-F/slot integrated dual-band four-antenna system for WLAN access point. *IEEE Ant. Wireless Prop. Lett.*, 14, 847–850.

[3] Zhang, L., Gao, S., Luo, Q., Young, P.R., Li, Q. (2017). Wideband loop antenna with electronically switchable circular polarization. *IEEE Ant. Wireless Prop. Lett*., 16, 242–245.

[4] Vendik, I.B., Rusakov, A., Kanjanasit, K., Hong, J., Filonov, D. (2017). Ultrawideband (UWB) planar antenna with single-, dual- and triple-band notched characteristic based on electric ring resonator. *IEEE Ant. Wireless Prop. Lett.*, 16, 1597–1600.

[5] Narbudowicz A., Amman, M.J. (2018). Low-cost multimode patch antenna for dual MIMO and enhanced localization use. *IEEE Trans. Ant. Prop*., 66(1), 405–408.

[6] Wu, J., Sarabandi, K. (2017). Compact omnidirectional circularly polarized antenna. *IEEE Trans. Ant. Prop.*, 65(4), 1550–1557.

[7] Balanis, C.A., (Editor), (2008). *Modern Antenna Handbook*. Wiley.

[8] Wei, D.J., Li, J., Yang, G., Liu, J., Yang, J.J. (2018). Design of compact dual-band SIW slotted array antenna. *IEEE Ant. Wireless Prop. Lett*., 17(6), 1085–1089.

[9] Zhu, S., Liu, H., Chen, Z., Wen, P. (2018). A compact gain-enhanced Vivaldi antenna array with suppressed mutual coupling for 5G mmwave application. *IEEE Ant. Wireless Prop. Lett.*, 17(5), 776–779.

[10] Koziel, S., Bekasiewicz, A. (2016). *Multi-objective design of antennas using surrogate models*. World Scientific.

[11] Wang, J., Yang, X.S., Ding, X., Wang, B.Z. (2017). Antenna radiation characteristics optimization by a hybrid topological method. *IEEE Trans. Ant. Prop.*, 65(6), 2843–2854.

[12] Kouassi, A., Nguyen-Trong, N., Kaufmann, T., Lallechere, S., Bonnet, P., Fumeaux, C. (2016). Reliability-aware optimization of a wideband antenna. *IEEE Trans. Ant. Prop.*, 64(2), 450–460.

Metrol. Meas. Syst., Vol. 26 (2019), No. 4, pp. 595–605
DOI: 10.24425/amms.2019.130561

[13] Choi, K., Jang, D.H., Kang, S.I., Lee, J.H., Chung, T K., Kim, H.S. (2016). Hybrid algorithm combining genetic algorithm with evolution strategy for antenna design. *IEEE Trans. Magn*., 52(3), 1–4.

[14] Zaharis, Z.D., Gravas, I.P., Yioultsis, T.V., Lazaridis, P.I., Glover, I.A., Skeberis, C., Xenos, T.D. (2017). Exponential log-periodic antenna design using improved particle swarm optimization with velocity mutation. *IEEE Trans. Magn*., 53(6), 1–4.

[15] Ghassemi, M., Bakr, M., Sangary, N. (2013). Antenna design exploiting adjoint sensitivity-based geometry evolution. *IET Microwaves Ant. Prop*., 7(4), 268–276.

[16] Xiao, L.Y., Shao, W., Ding, X., Wang, B.Z. (2018). Dynamic adjustment kernel extreme learning machine for microwave component design. *IEEE Trans. Microwave Theory Techn*., 66(10), 4452–4461.

[17] Koziel, S. Ogurtsov, S. (2014). *Antenna design by simulation-driven optimization. Surrogate-based approach*. Springer.

[18] de Villiers, D.I.L., Couckuyt, I., Dhaene, T. (2017). Multi-objective optimization of reflector antennas using kriging and probability of improvement. *Int. Symp. Ant. Prop.*, San Diego, USA, 985–986.

[19] Jacobs, J.P. (2016). Characterization by Gaussian processes of finite substrate size effects on gain patterns of microstrip antennas. *IET Microwaves Ant. Prop*., 10(11), 1189–1195.

[20] Zhu, J., Bandler, J.W., Nikolova, N.K., Koziel, S. (2007). Antenna optimization through space mapping. *IEEE Trans. Ant. Prop*., 55(3), 651–658.

[21] Koziel, S., Unnsteinsson, S.D. (2018). Expedited design closure of antennas by means of trust-region-based adaptive response scaling. *IEEE Ant. Wireless Prop. Lett.*, 17(6),1099–1103.

[22] Su, Y., Lin, J., Fan, Z., Chen, R. (2017). Shaping optimization of double reflector antenna based on manifold mapping. *Int. Applied Computational Electromagnetic Society Symp. (ACES)*, Suzhou, China, 1–2.

[23] Koziel, S. (2015). Fast simulation-driven antenna design using response-feature surrogates. *Int. J. RF & Micr. CAE*, 25(5), 394–402.

[24] Bekasiewicz, A., Koziel, S., Cheng, Q.S. (2018). Reduced-cost constrained miniaturization of wide-band antennas using improved trust-region gradient search with repair step. *IEEE Antennas Wireless Prop. Lett.*, 17(4), 559–562.

[25] Chen, Y.-C., Chen, S.-Y., Hsu, P. (2006). Dual-band slot dipole antenna fed by a coplanar waveguide. *IEEE Int. Symp. Ant. Prop*., Albuquerque, USA, 3589–3592.

[26] Alsath, M.G.N., Kanagasabai, M. (2015). Compact UWB monopole antenna for automotive communications. *IEEE Trans. Ant. Prop.*, 6(9), 4204–4208.

[27] Suryawanshi, D.R., Singh, B.A. (2014). A compact UWB rectangular slotted monopole antenna. *IEEE Int. Conf. Control, (ICCICCT)*, Kanyakumari, India, 1130–1136.

[28] Conn, A., Scheinberg, K., Vincente, L.N. (2009). *Introduction to Derivative-Free Optimization*. MPS-SIAM Series on Optimization.

[29] Nocedal, J., Wright, S. (2006). *Numerical Optimization*. 2nd ed., Springer.